J|A|C|S
ARTICLES
Published on Web 11/18/2003

The A-Cluster in Subunit β of the Acetyl-CoA Decarbonylase/Synthase Complex from *Methanosarcina thermophila*: Ni and Fe K-Edge XANES and EXAFS Analyses

Weiwei Gu,[†] Simonida Gencic,[§] Stephen P. Cramer,*[,†,‡] and David A. Grahame*[,§]

Contribution from the Physical Biosciences Division, Lawrence Berkeley National Laboratory, Berkeley, California 94720, Department of Applied Science, University of California, Davis, California 95616, and Department of Biochemistry and Molecular Biology, Uniformed Services University of the Health Sciences, Bethesda, Maryland 20814

Received June 10, 2003; E-mail: dgrahame@usuhs.mil

Abstract: The acetyl-CoA decarbonylase/synthase (ACDS) complex catalyzes the cleavage of acetyl-CoA in methanogens that metabolize acetate to CO_2 and CH_4, and also carries out acetyl-CoA synthesis during growth on one-carbon substrates. The ACDS complex contains five subunits, among which β possesses an Ni−Fe−S active-site metal cluster, the A-cluster, at which reaction with acetyl-CoA takes place, generating an acetyl-enzyme species poised for C−C bond cleavage. We have used Ni and Fe K fluorescence XANES and EXAFS analyses to characterize these metals in the ACDS β subunit, expressed as a C-terminally shortened form. Fe XANES and EXAFS confirmed the presence of an [Fe_4S_4] cluster, with typical Fe−S and Fe−Fe distances of 2.3 and 2.7 Å respectively. An Fe:Ni ratio of ~2:1 was found by K$\alpha\beta$ fluorescence analysis, indicating 2 Ni per [Fe_4S_4]. Ni XANES simulations were consistent with two distinct Ni sites in cluster A, and the observed spectrum could be modeled as the sum of separate square planar and tetrahedral Ni sites. Treatment of the β subunit with Ti^{3+} citrate resulted in shifts to lower energy, implying significant reduction of the [Fe_4S_4] center, along with conversion of a smaller fraction of Ni(II) to Ni(I). Reaction with CO in the presence of Ti^{3+} citrate generated a unique Ni XANES spectrum, while effects on the Fe-edge were not very different from the reaction with Ti^{3+} alone. Ni EXAFS revealed an average Ni coordination of 2.5 S at 2.19 Å and 1.5 N/O at 1.89 Å. A distinct feature at ~2.95 Å most likely results from Ni−Ni interaction. The methanogen β subunit A-cluster is proposed to consist of an [Fe_4S_4] cluster bridged to an Ni−Ni center with one Ni in square planar geometry coordinated by 2 S + 2 N and the other approximately tetrahedral with 3 S + 1 N/O ligands. The electronic consequences of two distinct Ni geometries are discussed.

Introduction

Cleavage of the C−C bond of acetate is a critical step in the metabolism of acetate to CO_2 and methane carried out by species of methanogenic Archaea.[1,2] Acetate is first converted to acetyl-CoA, and then the acetate C−C bond is broken by a metal-based decarbonylation reaction catalyzed by a multi-enzyme complex designated acetyl-CoA decarbonylase/synthase (ACDS). The ACDS complex constitutes as much as 25% of the soluble protein in *Methanosarcina thermophila* growing on acetate as sole source of carbon and energy, and also may function at lower levels in the reverse direction for assimilation of carbon in methanogens growing on C-1 substrates. Anaerobic species of sulfate-reducing Archaea also use high levels of ACDS for acetate cleavage,[3,4] with subsequent oxidation of both acetate carbons to CO_2.

The ACDS complex is composed of five different subunits in an $(\alpha_2\epsilon_2)_4\beta_8(\gamma\delta)_8$ oligomeric structure with an overall molecular mass of about 2,000 kDa, and catalyzes reaction 1:[5]

$$\text{Acetyl-CoA} + H_4\text{SPt} + H_2O \rightleftarrows \text{CoASH} + CH_3{-}H_4\text{SPt} + CO_2 + 2H^+ + 2e^- \quad (1)$$

where H_4SPt and CH_3-H_4SPt stand for the H_4-folate analogues tetrahydrosarcinapterin and N^5-methyltetrahydrosarcinapterin, respectively. Studies on protein components of the ACDS complex, separated by ion-exchange chromatography after dissociation of the native complex by limited proteolysis, showed that an acetyl-enzyme species is formed on the β subunit, which contains Ni and an Fe−S center, in a reaction

[‡] Lawrence Berkeley National Laboratory.
[†] University of California.
[§] Uniformed Services University of the Health Sciences.

(1) Alber, B. E.; Clements, A. P.; Jablonsky, P. E.; Latimer, M. T.; Ferry, J. G., In *Microbial Growth on C1 Compounds*; Murrell, J. C. and Kelly, D. P., Ed.; Intercept Ltd.: Andover, UK, 1993; pp 163−170.
(2) Ferry, J. G., In *Methanogenesis: Ecology, Physiology, Biochemistry & Genetics*; Ferry, J. G., Ed.; Chapman & Hall: New York, 1993; pp 304−334.
(3) Thauer, R. K. In *Autotrophic Bacteria*; Schlegel, H. G., Bowien, B., Eds.; Science Tech Publishers: Springer-Verlag: Madison, WI, and Berlin, New York, 1989; pp 397−413.
(4) Dai, Y.-R.; Reed, D. W.; Millstein, J. H.; Hartzell, P. L.; Grahame, D. A.; DeMoll, E. *Arch. Microbiol.* **1998**, *169*, 525−529.
(5) Grahame, D. A. *J. Biol. Chem.* **1991**, *266*, 22227−22233.

with acetyl-CoA that is strictly dependent on low redox potential ($E^{\circ}_{app} = -486$ mV, pH 6.5), according to reaction 2.[6,7]

$$E_{\beta} + \text{acetyl-CoA} \rightleftarrows E_{\beta}\text{-acetyl} + \text{CoA} \qquad K'_{eq} = 0.15-0.27 \quad (2)$$

A large negative value was indicated for the standard free energy of hydrolysis of the acetyl-enzyme (−9.3 to −9.6 kcal/mol), and this "high energy" acetyl intermediate has been proposed to be the proximal species undergoing C−C bond fragmentation.[7]

Recently, Ni-free recombinant β subunit preparations have been obtained, following expression in *Escherichia coli* under anaerobic conditions, that contain an Fe−S center and can be reconstituted with $NiCl_2$. The reconstituted protein exhibited redox properties and enzymatic activity matching that of the native subunit following its isolation from other subunits of the ACDS complex.[8] Net synthesis of acetyl-CoA from CO, CoA, and methylcobalamin in the absence of all other ACDS proteins demonstrated unequivocally that the active site for C−C bond formation/cleavage resides on the β subunit. Metal analyses on Ni-reconstituted and native forms of the β subunit indicated an Fe:Ni stoichiometry close to 2:1, consistent with a protein containing one $[Fe_4S_4]$ cluster and two Ni. The recombinant β subunit reacted with CO to form a stable EPR-detectable adduct, exhibiting paramagnetic properties characteristic of a unique heterometallic center known as the A-cluster. The A-cluster EPR signal has been observed for the intact ACDS complex from Archaea[9,10] and for the 310 kDa $\alpha_2\beta_2$ bifunctional enzyme CO dehydrogenase/acetyl-CoA synthase (CODH/ACS) from the bacterium *Moorella thermoacetica*, in which the A-cluster is located in the homologous α subunit.[11−14] In the methanogen β subunit, UV−visible spectroscopic studies indicated multiple thiolate ligation to Ni in the A-cluster, and site-directed mutagenesis experiments implicated the conserved cysteine residues Cys 278 and Cys 280 as ligands to Ni.[8]

Recently, two crystal structures of *M. thermoacetica* CODH/ACS have been reported.[15,16] Both contain A-cluster structures with an $[Fe_4S_4]$ unit bridged by a cysteine thiolate to a binuclear metal center containing at least one Ni. Differences existed in the identity and structural characteristics of the other metal in the binuclear center. In the first report, a distorted tetrahedral Cu was observed at the binuclear site M_a, proximal to the $[Fe_4S_4]$ cluster, and subsequent X-ray absorption analysis showed this to be Cu(I).[17] The distal site, M_b, contained Ni in square planar geometry coordinated by two amide nitrogens from the protein backbone and by two cysteine thiolates, corresponding to Cys 278 and Cys 280 in the ACDS β subunit. The second CODH/ACS structure, obtained under different crystallization conditions, revealed differences in the protein conformations for the two α subunits, one designated "open" with greater solvent accessibility to the A-cluster and the other "closed" with lower exposure to solvent.[16] In agreement with the first reported structure, both A-cluster forms contained square planar Ni at the distal site. However, in the open form the proximal metal site was occupied by a distorted square planar Ni, in an $[Fe_4S_4]$−Ni−Ni arrangement, whereas in the closed form this site contained Zn in tetrahedral geometry, an $[Fe_4S_4]$−Zn−Ni type. Since neither Cu nor Zn was found at significant levels in the methanogen β subunit, a binuclear Ni−Ni site in the A-cluster of the ACDS complex was proposed.[8]

K-edge X-ray absorption spectroscopy has been used as a probe of the Ni in CODH/ACS as early as 1987,[14,18−20] although the initial work was not cognizant of the multiplicity of Ni sites. To simplify the analyses, later studies either employed CODH enzymes that contained only the CO activating C-clusters,[21] or isolated α subunits that contained only A-clusters.[14,20] From the latter studies, the coordination environment of the A-cluster Ni site was deduced to involve distorted square planar geometry with 2 S ligands at 2.19 Å and 2 N/O atoms at 1.89 Å.[14,20] More recent L-edge spectroscopy of the $\alpha_2\beta_2$ CODH/ACS yielded evidence for a mixture of high-spin and low-spin Ni(II) species,[22] but the source of this heterogeneity remained ambiguous.

As yet, X-ray spectroscopic methods have not been applied to study the A-cluster in the methanogen ACDS β subunit. Therefore, a series of investigations were carried out to characterize the metals in the β subunit A-cluster using a variety of X-ray spectroscopic techniques. In the present contribution we report Ni and Fe K-edge XANES and EXAFS analyses of the methanogen β subunit metalloprotein. The results are interpreted in light of the recent crystal structures of CODH/ACS, and along with companion studies using L-edge X-ray absorption and X-ray magnetic circular dichroism (XMCD) spectroscopy.[23]

Experimental Procedures

Preparation and Assay of Protein Samples. The β subunit of the ACDS complex of *Methanosarcina thermophila* strain TM-1 was expressed in *E. coli* grown under strictly anaerobic conditions in a form containing 397 amino acids, designated CdhC*. This protein is 75 amino acids shorter than the full-length protein, and it was designed to mimic the C-terminally truncated β subunit isolated following proteolytic dissociation of the ACDS complex. Preparation of an expression vector construct, expression in *E. coli* under anaerobic growth conditions, and

(6) Grahame, D. A.; DeMoll, E. *J. Biol. Chem.*, **1996**, *271*, 8352−8358.
(7) Bhaskar, B.; DeMoll, E.; Grahame, D. A. *Biochemistry* **1998**, *37*, 14491−14499.
(8) Gencic, S.; Grahame, D. A. *J. Biol. Chem.* **2003**, *278*, 6101−6110.
(9) Terlesky, K. C.; Barber, M. J.; Aceti, D. J.; Ferry, J. G. *J. Bacteriol.* **1987**, *262*, 15392−15395.
(10) Grahame, D. A.; Khangulov, S.; DeMoll, E. *Biochemistry* **1996**, *35*, 593−600.
(11) Ragsdale, S. W.; Ljungdahl, L. G.; DerVartanian, D. V. *Biochem. Biophys. Res. Commun.* **1983**, *115*, 685−665.
(12) Ragsdale, S. W.; Wood, H. G.; Antholine, W. E. *Proc. Natl. Acad. Sci. U.S.A.*, **1985**, *82*, 6811−6814.
(13) Lindahl, P. A.; Münck, E.; Ragsdale, S. W. *J. Biol. Chem.* **1990**, *265*, 3873−3879.
(14) Xia, J.; Dong, J.; Wang, S.; Scott, R. A.; Lindahl, P. A. *J. Am. Chem. Soc.* **1995**, *117*, 7065−7070.
(15) Doukov, T. I.; Iverson, T. M.; Seravalli, J.; Ragsdale, S. W.; Drennan, C. L. *Science* **2002**, *298*, 567−572.
(16) Darnault, C.; Volbeda, A.; Kim, E. J.; Legrand, P.; Vernéede, X.; Lindahl, P. A.; Fontecilla-Camps, J. C. *Nat. Struct. Biol.* **2003**, *4*, 271−279.
(17) Seravalli, J.; Gu, W.; Tam, A.; Strauss, E.; Begley, T. P.; Cramer, S. P.; Ragsdale, S. W. *Proc. Natl. Acad. Sci. U.S.A.* **2003**, *100*, 3689−3694.
(18) Cramer, S. P.; Eidsness, M. K.; Pan, W.-H.; Morton, T. A.; Ragsdale, S. W.; DerVartanian, D. V.; Ljungdahl, L. G.; Scott, R. A. *Inorg. Chem.* **1987**, *26*, 2477−2479.
(19) Bastian, N. R.; Diekert, G.; Niederhoffer, E. C.; Teo, B.-K.; Walsh, C. T.; Orme-Johnson, W. H. *J. Am. Chem. Soc.* **1988**, *110*, 5581−5582.
(20) Russell, W. K.; Stålhandske, C. M. V.; Xia, J.; Scott, R. A.; Lindahl, P. A. *J. Am. Chem. Soc.* **1998**, *120*, 7502−7510.
(21) Tan, G. O.; Ensign, S. A.; Ciurli, S.; Scott, M. J.; Hedman, B.; Holm, R. H.; Ludden, P. W.; Korsun, Z. R.; Stephens, P. J.; Hodgson, K. O. *Proc. Natl. Acad. Sci. U.S.A.* **1992**, *89*, 4427−4431.
(22) Ralston, C. Y.; Wang, H.; Ragsdale, S. W.; Kumar, M.; Spangler, N. J.; Ludden, P. W.; Gu, W.; Jones, R. M.; Patil, D. S.; Cramer, S. P. *J. Am. Chem. Soc.* **2000**, *122*, 10553−10560.
(23) Funk, T.; Gu, W.; Friedrich, S.; Wang, H.; Grahame, D. A.; Cramer, S. P. *J. Am. Chem. Soc.* **2003**, *125*. In press..

subsequent purification of the protein by ion-exchange chromatography were performed as described previously.[8] All procedures used for purification and preparation of samples for EXAFS measurements were performed under anaerobic conditions inside a Coy-type anaerobic chamber with O_2 levels in the range of 0.5−2.0 ppm monitored continuously with a calibrated Teledyne model 3190 trace oxygen analyzer.

The purified protein, containing an Fe−S center but lacking Ni, was reconstituted by incubation with $NiCl_2$ followed by removal of excess Ni by ultrafiltration and subsequent gel filtration on Sephadex G-25, as previously described.[8] Protein concentration of samples for EXAFS was 1.2−1.7 mM as measured by a method using absorbance at 280 nm (described in ref 8), which agrees with protein dye-binding assays using BSA as standard. ICP analyses yielded Fe contents of 3.0 ± 0.2 g atom/mol protein and the protein is estimated to be 90−93% pure on the basis of densitometry of SDS gels. The Fe/Ni ratio was 1.8−1.9, as measured by direct ICP analyses of the Ni-reconstituted protein and by $NiCl_2$ titration of the apoprotein, respectively. Moreover, all apoprotein preparations exhibited a highly consistent value of the $A_{280}/A_{400\ nm}$ ratio of 5.11 ± 0.05 (n = 4). Samples for EXAFS contained 0.9−1.3 mM CdhC*, determined on the basis of one-fourth of the iron content, and were prepared by ultrafiltration on Centricon 30 concentrators (Millipore, Corp.) to concentrate the protein. Glycerol was added to a final concentration of 20% v/v and the samples were transferred to EXAFS cells and frozen by immersion in liquid N_2. For reduction of the enzyme, stock solutions of 140 mM Ti^{3+} citrate were prepared immediately before use as described in ref 7, and diluted with 25 mM HEPES, pH 7.2, to give working solutions containing 42 mM Ti^{3+}. Concentrated protein samples containing glycerol were reduced in the presence of 3 mM Ti^{3+} citrate, obtained by addition of an appropriate volume of the Ti^{3+} working solution, and incubated at room temperature for 20 min prior to freezing. These samples are referred to as "Ti^{3+}-reduced", whereas samples containing no Ti^{3+} are designated "as-isolated". Samples for reaction with CO were prepared identically, except that incubation with Ti^{3+} was carried out for 25 min along with gentle agitation under an atmosphere of 100% CO (Matheson, research grade, >99.99%), designated "Ti^{3+}/CO", or for 30 min in the absence of Ti^{3+}, "CO-only". Following X-ray absorption measurements, the samples were thawed, and enzymatic assays for acetyltransferase activity were performed as described previously.[8] Recovered activity was 60% in the as-isolated samples in the absence of CO, and 65% in its presence, with 100% activity corresponding to a turnover rate for acetyl transfer of 4500 min^{-1}. The lowest recovery, 13%, was observed in Ti^{3+}-reduced samples, but was significantly higher, around 48% in the Ti^{3+}/CO samples.

Model Compounds. The square planar Ni complex (nBu$_4$N)[Ni(tfd)$_2$] (tfd = *cis*-trifluoromethylethylene-1,2-dithiolato)[24] was prepared in the laboratory of Dr. Edward I. Stiefel, Princeton University, Princeton, NJ, and the tetrahedral Ni complex PhTt(tBu)NiCl, where PhTt(tBu) represents phenyl-tris((*tert*-butylthio)methyl)borate,[25] was prepared in the laboratory of Dr. Charles G. Riordan, University of Delaware, Newark, DE, both using the cited literature methods.

Metal Content. The X-ray fluorescence spectra for metal analyses were recorded at beam lines 7-3 and 9-3 at the Stanford Synchrotron Radiation Laboratory (SSRL) at a fixed excitation energy of 10 keV. The fluorescence intensities were obtained by integration of Gaussian curves that gave the best least-squares fit to the data. To correct for different fluorescence yields and detector efficiencies for different fluorescence lines, samples with known Fe:Ni ratios were used as standards: *M. thermoacetica* CODH/ACS (7:1 Fe:Ni ratio),[15] *Carboxydothermus hydrogenoformans* CODH (10:1 Fe:Ni ratio)[26] and *Ralstonia eutropha* NAD^+-reducing hydrogenase (19:1 Fe:Ni ratio).[27] The Fe:Ni Kα fluorescence intensity ratios obtained for these samples were then used to construct a standard curve of Fe:Ni Kα ratio vs Fe:Ni composition. Data were collected with two channels of a Canberra 30-element Ge detector and Canberra 2026 amplifiers using 0.125 μs shaping times. The total count rate for each detector was about 80 000 cps. The collection time for each sample was 10 min. A Canberra AIM 556A multichannel analyzer was used to record the X-ray fluorescence spectra.

XAFS Measurements. Ni and Fe K-edge spectra were recorded at beam lines 7-3 and 9-3 at SSRL using Si(220) monochromator crystals. The energy was calibrated using either a Ni or Fe foil as an internal standard in a three-ion chamber geometry, setting the first inflection point of the Ni and Fe foil spectra to 8331.6 and 7112.0 eV, respectively. All ion chambers were filled with N_2. Harmonic rejection at beamline 7-3 was accomplished by detuning the second monochromator crystal to 50% of the maximum possible flux. At beamline 9-3, the beam was fully tuned, and a harmonic rejection mirror with energy cut off at 11 keV was used. During all X-ray measurements, the samples were maintained at a temperature of ~10 K using an Oxford Instruments CF1208 helium flow cryostat. To reduce radiation damage, the enzyme samples were moved relative to the incident beam position after every fourth scan. The energy of the Ni K-edge and the Fe K-edge of the enzyme was monitored on sequential scans to confirm the integrity of the enzyme in the X-ray beam.

Fluorescence-detected absorption spectra were recorded using a Canberra 30-element Ge detector with the same model Canberra amplifiers and shaping times mentioned previously. Single channel analyzers were used to set electronic windows around the Ni or Fe Kα fluorescence. The average Ni (Fe) signal count rate at each individual detector element was ~5000 (7000) cps, while the total count rates were on the order of 80 000 cps at the end of each scan.

XANES Simulations. XANES spectra were calculated using FEFF, version 8.20[28] on a 1 GHz Apple G4 computer. The self-consistent muffin-tin potential and full multiple scattering (FMS) calculations were determined with about 80 atoms for synthetic model complexes and 64 atoms for the protein. A −3 eV shift was added to the calculated spectra to correct the potential. XANES spectra of the model compounds were calculated using the known crystal coordinates.[25] The coordinates used for the enzyme calculations were adapted from the crystal structure of the A-cluster for *M. thermoacetica* CODH/ACS.[15] The XANES spectrum of the α subunit was digitized from literature.[14]

EXAFS Analyses. The Ni or Fe EXAFS signals were extracted from the averaged excitation spectra using EXAFSPAK software,[29] using 8350 or 7130 eV respectively, as an initial E_o for defining the photoelectron wavenumber k. Least-squares fits of the EXAFS data $\chi(k)$ were performed using Fourier-filtered data, using the following approximate formula to optimize the structural parameters N_b, R_{ab}, and σ_{ab}^2:

$$\chi(k) = S_0^2(k)\sum_b (N_b/kR_{ab}^2)|f_b(k)|\, e^{-2\sigma_{ab}^2k^2} e^{-2R_{ab}/\lambda(k)} \sin[2kR_{ab} + \phi_{ab}(k)]$$

In this equation, N_b is the number of backscatterers in the bth backscattering shell at distance R_{ab} from the X-ray absorber a, $f_b(k)$ and $\phi_{ab}(k)$ are the backscattering amplitude and total phase-shift of the absorber-scatterer pairs, respectively, σ_{ab}^2 is the mean square deviation of R_{ab}, and $\lambda(k)$ represents the mean free path of the ejected photoelectron. $S_0^2(k)$ is an amplitude reduction factor that accounts for

(24) Davison, A.; Holm, R. H. *Inorg. Synth.* **1967**, *10*, 8−27.
(25) Schebler, P. J.; Riordan, C. G.; Guzei, I. A.; Rheingold, A. L. *Inorg. Chem.* **1998**, *37*, 4754−4755.
(26) Dobbek, H.; Svetlitchnyi, V.; Gremer, L.; Huber, R.; Meyer, O. *Science* **2001**, *293*, 1281−1285.
(27) Massanz, C.; Schmidt, S.; Friedrich, B. *J. Bacteriol.* **1998**, *180*, 1023−1029.
(28) Ankudinov, A. L.; Ravel, B.; Rehr, J. J.; Conradson, S. D. *Phys. Rev. B: Condens. Matter* **1998**, *58*, 7565−7576.
(29) The EXAFSPAK is a suite of XAS data analysis programs developed by Dr. G. N. George of SSRL available at http://www-ssrl.slac.stanford.edu/exafspak.html.

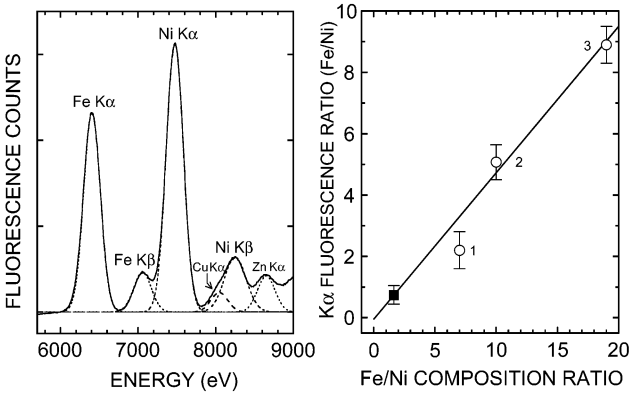

Figure 1. Metal content analysis using Kαβ fluorescence. (Left) X-ray fluorescence spectrum of ACDS β subunit at an excitation energy of 10 keV, solid line. Gaussian fits to components are shown as broken lines. (Right) Calibration curve plotted for the observed Fe/Ni Kα fluorescence ratio vs Fe/Ni composition ratio in proteins. Standard proteins were, (1) *Morella thermoacetica* CODH/ACS, (2) *Rhodospirillum rubrum* carbon monoxide dehydrogenase, and (3) *Ralstonia eutropha* NAD^+-reducing hydrogenase. The ACDS β subunit is indicated (■). A linear least-squares fit is shown (—) obtained by using all four points, with theoretical Fe/Ni values of 4.67, 10, 19, and 2, respectively.

multielectron excitations. The functions $f_b(k)$, $\phi_{ab}(k)$, and $\lambda(k)$ were calculated using the program FEFF 7.01.[30] The goodness of fit F was determined by

$$F = \sum_i [\chi(k_i)_{\text{calc}} - \chi(k_i)_{\text{obs}}]^2 k^6$$

Results and Discussion

Metal Content. The Fe:Ni ratio in the β subunit (CdhC*) was determined by X-ray fluorescence spectroscopy using the relative intensities of Fe and Ni K fluorescence signals compared with standard proteins containing Ni and Fe (Figure 1). The β subunit Fe/Ni ratio was estimated to be 1.7 ± 0.3, indicating a stoichiometry of 2 Ni per $[Fe_4S_4]$ cluster, in agreement with metal analyses carried out previously by different methods.[8] The X-ray fluorescence spectrum also revealed that Cu and Zn were not present in significant amounts in the β subunit (<0.02 Cu per Ni, <0.03 Zn per Ni),[31] which also agrees with previous studies on the native and recombinant β subunit, but stands in contrast to the recent crystal structures of *M. thermoacetica* CODH/ACS, where other metals, Cu[15] or Zn[16] were indicated to be stoichiometric components of the A-cluster. Notably, CODH/ACS showed a substantial deviation (Figure 1, right) from the linear relationship of Fe/Ni K fluorescence to protein Fe/Ni composition. The extent of deviation was outside the expected range of experimental error, suggesting a substantially lower Fe:Ni composition than would be expected for that protein containing an A-cluster with only one Ni.

XANES Spectra. The Fe and Ni K-edge spectra are shown in Figure 2 for the as-isolated β subunit, and are compared with the spectra obtained after reaction of the enzyme with CO or after treatment with Ti^{3+} in the presence or absence of CO. The Fe K-edge exhibited a strong "1s → 3d" transition at ~7112 eV, consistent with tetrahedral Fe coordination.[32] Fe K-edge data were recorded for two samples of the as-isolated protein. Both of these exhibited a major inflection point at 7117.5 eV, which agrees with the value expected for an $[Fe_4S_4]^{2+}$ cluster.[33] Reaction with CO by itself showed almost no change in the Fe-edge spectrum. By contrast, the first major inflection point shifted to lower energy by 0.14 to 0.48 eV in samples reduced with Ti^{3+} citrate, while a shift of 0.23 eV was observed for the Ti^{3+}/CO sample (Figure 2A). A shift of 0.4 eV has been observed for the $[Fe_4S_4]^{2+} \rightarrow [Fe_4S_4]^{1+}$ conversion, and a 0.7 eV shift was observed for creation of the "all-ferrous" $[Fe_4S_4]^0$ form.[33] Assuming that such shifts are general for $[Fe_4S_4]^{n+}$ clusters, the changes that we observe would be consistent with 50 to 100% conversion to the $[Fe_4S_4]^{1+}$ state.

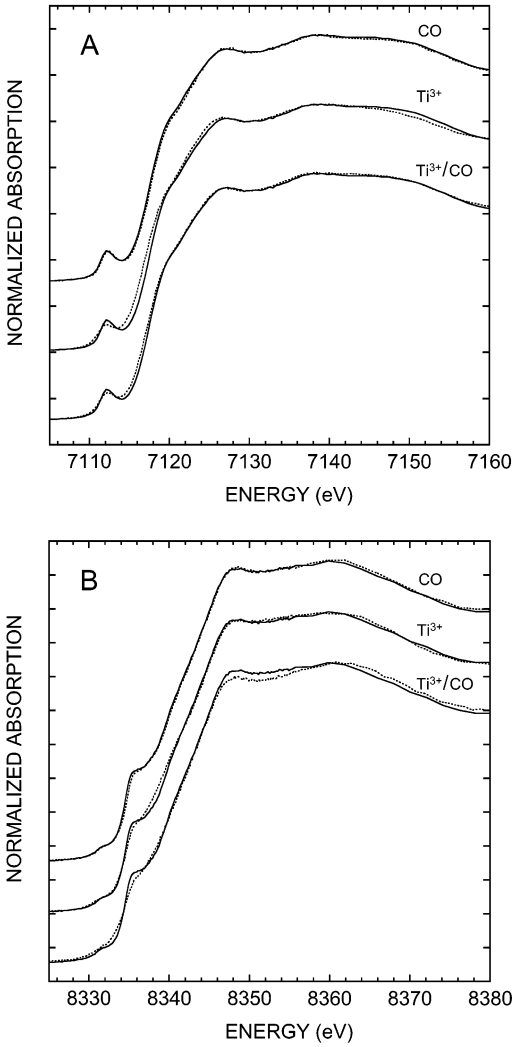

Figure 2. Fe and Ni K-edge XANES spectra of the ACDS β subunit and the effects of exposure to CO, Ti^{3+} citrate, and Ti^{3+} citrate plus CO. Normalized Fe **(**A**)** and Ni **(B)** K-edge XANES spectra of the β subunit as-isolated (—) are compared with the spectra obtained following incubation under 1 atm CO, or with 3 mM Ti^{3+} citrate, or with 3 mM Ti^{3+} plus CO, as indicated (- - -).

(30) Ankudinov, A. L.; Rehr, J. J. *Phys. Rev. B: Condens. Matter* **1997**, *56*, R1712−R1716.

(31) K fluorescence peak intensities are highly energy- and element-dependent. They are enhanced by larger absorption cross sections, higher fluorescence yields, and greater fluorescence transmission, all of which occur for higher Z elements. Thus, the relatively large Cu and Zn peak areas actually correspond to less than 2 and 3% of the Ni content, respectively (on the basis of analysis of separate Cu and Zn standards, not shown). Similarly, the observed Ni peak area is notably larger than the Fe peak, even though the Fe content is approximately twice that of Ni.

(32) Westre, T. E.; Kennepohl, P.; DeWitt, J. G.; Hedman, B.; Hodgson, K. O.; Solomon, E. I. *J. Am. Chem. Soc.* **1997**, *119*, 6297−6314.

(33) Musgrave, K. B.; Angove, H. C.; Burgess, B. K.; Hedman, B.; Hodgson, K. O. *J. Am. Chem. Soc.* **1998**, *120*, 5325−5326.

Two characteristic preedge transitions were observed in Ni K-edge spectra of the β subunit − a weak "1s → 3d" transition at 8331 eV and a stronger "1s → $4p_z$" feature at ∼8336 eV (Figure 2B). Ni K-edge data were recorded on three samples of the as-isolated protein. The average value of the major inflection point was 8340.7 eV, and all three were within ±0.2 eV of this value. The value of 8340.7 eV is consistent with a Ni(II) assignment.[34−37] There was almost no change in the position of this point in the presence of CO alone, analogous to the results seen at the Fe-edge. However, samples treated with Ti^{3+} were shifted to lower energy from 0.2 to 0.6 eV. In comparison with the as-isolated protein, the "1s → $4p_z$" transition was slightly weaker for the Ti^{3+}-treated and weakest for the Ti^{3+}/CO form. Typical shifts between Ni(II) and Ni(I) are on the order of 2 eV.[34−37] Thus, the observed changes may result from a modest change in geometry at one or both Ni sites, and/or a reduction of a fraction (at most ∼50%) of the Ni to Ni(I) or Ni(0). We note that a Ni(I) fraction also was observed in the Ti^{3+}-treated samples prepared for L-edge analysis.[23]

The spectrum of the Ti^{3+}/CO treated enzyme was different from all other samples. As mentioned above, this form displays the weakest "1s → $4p_z$" transition of all. In addition, a second derivative zero crossing in the 8338 to 8342 eV region was not found and, as shown in Figure 2B, the intensity of the near-edge feature around 8349 eV was notably decreased. Two such Ti^{3+}/CO samples were measured, and both showed very similar results.

Using previously described normalization procedures,[34,38,39] the normalized integrated intensities of "1s → 3d" transition for as-isolated and Ti^{3+}-treated ACDS β subunit were 0.031 and 0.029 eV, respectively. Square planar Ni(II) complexes are reported to have normalized integrated areas of 0.005−0.029 eV, while tetrahedral complexes have much stronger transitions with areas of 0.080−0.114 eV, due to p−d mixing.[34] Given the range of reported intensities, one can exclude purely tetrahedral coordination as the average geometry for the Ni centers, but a wide range of distorted square planar and distorted tetrahedral combinations remain possible.

The β subunit Ni K-edge features were interpreted in view of the evidence for heterogeneous A-cluster Ni sites in CODH/ACS, i.e., chemical (labile vs nonlabile),[20,40] crystallographic (tetrahedral vs square planar),[15,16] and L-edge spectroscopic (high-spin vs low-spin).[22,23] Previously, the K-edge of the CODH/ACS α metallosubunit − which contains nonlabile Ni, presumably corresponding to the distal Ni site − was considered as evidence for a distorted square planar geometry,[14,20] with a dihedral angle of 20−30° [14] or greater.[20] This interpretation was based on the observation that the "1s → $4p_z$" intensity in four-coordinate NiL_2X_2 compounds is sensitive to the dihedral angle φ defined by L−Ni−X and L′−Ni−X′, and that larger values of φ correspond to less "1s → $4p_z$" and more "1s → 3d" intensity.[14] However, instead of invoking a distorted square planar geometry, a more satisfactory interpretation now comes from the assumption of two different Ni geometries (tetrahedral and square planar), consistent with the recent crystallographic studies.

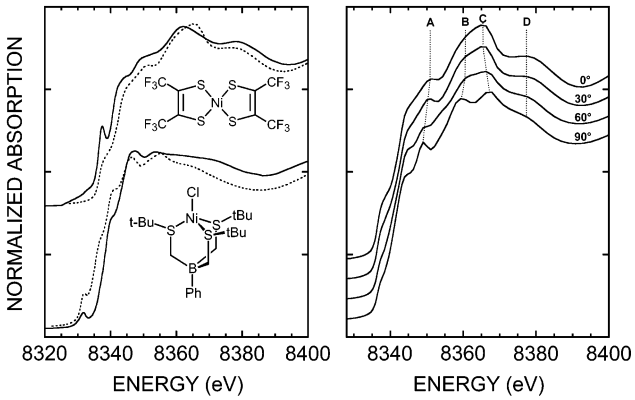

Figure 3. Comparison of the observed and theoretically calculated Ni XANES spectra of square planar and tetrahedral Ni model compounds using FEFF8. (Left) Experimentally measured Ni XANES spectra (—) and FEFF8 simulations (- - -) of $(Bu_4N)Ni(tfd)_2$ (top) and PhTt(*t*Bu)NiCl (bottom) with structures as shown. (Right) FEFF8-calculated XANES spectra of $Ni(tfd)_2$ obtained by distorting the dihedral angle φ defined by S_1-Ni-S_2 and S_3-Ni-S_4 in 30° increments from 0° (square planar) to 90° (tetrahedral).

Ni XANES Simulations. To model the β subunit K-edge spectrum both theoretically and experimentally as the sum of separate spectra arising from two distinct Ni sites, we first conducted FEFF8 simulations for two model compounds with the appropriate geometries, the square planar Ni complex $(nBu_4N)[Ni(tfd)_2]$[24,25] and PhTt(*t*Bu)NiCl, with a tetrahedral Ni site.[25] Using the crystal structure coordinates,[25,41] even without any geometry optimization, the FEFF8 calculations reproduced rather well the higher-energy portion of the experimental XANES spectra (Figure 3, left). The agreement for the "1s → 3d" and "1s → $4p_z$" transitions was less quantitative, and further theoretical development or optimization may be needed for these lower-energy features. Nevertheless, it is clear that, given the correct molecular structures, FEFF8 calculations provide good simulations of the overall shape of the XANES spectra.

FEFF8 was also used to examine how geometric distortions might affect the XANES spectra. The structure for the $[Ni(tfd)_2]^-$ anion was modified by twisting the dihedral angle φ between the S_1-Ni-S_2 and S_3-Ni-S_4 planes in 30° increments, from the original square planar geometry to a final tetrahedral Ni center, and FEFF8 calculations were done for each structure (Figure 3, right). In the higher-energy region between 8345 and 8385 eV, there are four distinct features (labeled A, B, C, and D in Figure 3) that exhibited gradual changes in energy and intensity as φ was increased from 0 to 90°. Specifically, in tetrahedral geometry a relatively sharp peak emerged at low energy (∼8348 eV), almost exactly where distinct features are observed in the tetrahedral PhTt(*t*Bu)NiCl model compound as well as in the ACDS β subunit Ni spectrum. Overall, the simulations provided further evidence that distortions in geom-

(34) Colpas, G. J.; Maroney, M. J.; Bagyinka, C.; Kumar, M.; Willis, W. S.; Suib, S. L.; Baidya, N.; Mascharak, P. K. *Inorg. Chem.* **1991**, *30*, 920−928.
(35) Smith, M. C.; Barclay, J. E.; Cramer, S. P.; Davies, S. C.; Gu, W.; Hughes, D. L.; Longhurst, S.; Evans, D. J. *J. Chem. Soc., Dalton Trans.* **2002**, 2641−2647.
(36) Mandimutsira, B. S.; Yamarik, J. L.; Brunold, T. C.; Gu, W.; Cramer, S. P.; Riordan, C. G. *J. Am. Chem. Soc.* **2001**, *123*, 9194−9195.
(37) Gu, W.; Jacquamet, L.; Patil, D. S.; Wang, H.-X.; Evans, D. J.; Smith, M. C.; Millar, M.; Koch, S.; Eichhorn, D. M.; Latimer, M.; Cramer, S. P. *J. Inorg. Biochem.* **2003**, *93*, 41−51.
(38) Eidsness, M. K.; Sullivan, R. J.; Scott, R. A. In *The Bioinorganic Chemistry of Nickel*; Lancaster, J. R., Jr., Ed.; VCH Publishers: New York, 1988; pp 73−91.
(39) Bagyinka, C.; Whitehead, J. P.; Maroney, M. J. *J. Am. Chem. Soc.* **1993**, *115*, 3576−3585.
(40) Xia, J.; Hu, Z.; Popescu, C. V.; Lindahl, P. A.; Münck, E. *J. Am. Chem. Soc.* **1997**, *119*, 8301−8312.
(41) Singhabhandhu, A.; Robinson, P. D.; Fang, J. H.; Geiger, W. E., Jr. *Inorg. Chem.* **1975**, *14*, 318−323.

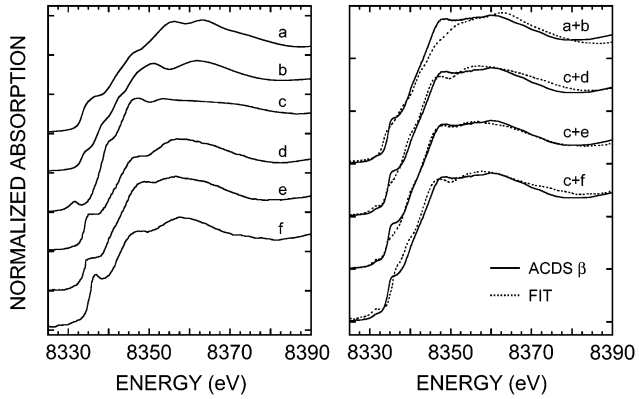

Figure 4. As-isolated β subunit Ni XANES spectrum modeled as the sum of separate square planar and tetrahedral Ni sites. (Left) spectra used for fitting procedures: **a** square planar and **b** tetrahedral sites calculated theoretically using FEFF8; **c** spectrum measured for the tetrahedral model compound PhTt(*t*Bu)NiCl; **d** and **e** literature spectra of the CODH/ACS α subunit without[14] and with treatment with 1,10-phenanthroline,[20] respectively; **f** measured spectrum of the square planar complex $(Bu_4N)[TrisFe_4S_4NiN_2S_2]$.[42] (Right) observed spectrum of the as-isolated ACDS β subunit (—) and fits (- - -) obtained using the following model spectra: **a**+**b** (50% a + 50% b); **c**+**d** (50% c + 50% d); **c**+**e** (40% c + 60% e); **c**+**f** (50% c + 50% f).

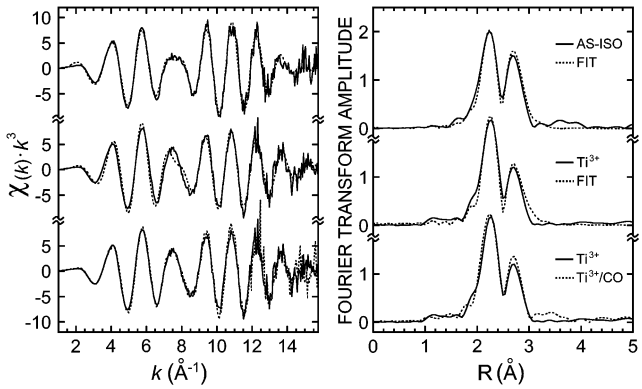

Figure 5. Fe *k*-space EXAFS and Fourier transforms for the ACDS β subunit. (Left) EXAFS spectra (—) and best fits (- - -) for samples: as-isolated, top; Ti^{3+} reduced, middle; and Ti^{3+}/CO treated, bottom. (Right) Fourier transformed EXAFS spectra (—) and best fits (- - -) of the as-isolated, top; and Ti^{3+} reduced samples, middle. A comparison of the Ti^{3+} reduced (—) and Ti^{3+}/CO treated forms (- - -) is shown, bottom. The Fourier transform range was $k = 1-15.0$ Å^{-1}.

etry not only change the preedge peak intensities, as observed in previous XAS experiments, but affect the higher-energy XANES features as well.

Theoretical simulation of the Ni XANES spectrum of the ACDS β subunit was then carried out using coordinates from the first CODH/ACS crystal structure.[15] A square planar Ni structure was taken directly from the PDB file and used for the coordinates for the distal Ni_b site, and a tetrahedral Ni_a site was obtained by replacing the Cu atom at the proximal M_a site with Ni. A water molecule was used as the undefined fourth ligand to M_a. The resulting simulations for the two sites are shown in Figure 4, left. The calculated spectrum for the square planar site (Figure 4, left **a**) has a weak transition at 8349 eV but a strong transition at 8355 eV, while the opposite is seen for the tetrahedral site (Figure 4, left **b**). Neither of these individual calculated spectra adequately modeled the experimental data. However, an average of these two spectra produced a spectrum that was a significantly better simulation (Figure 4, right **a**+**b**). Although these results were consistent with a two-site model, improvements in the quality of the simulation were desired, and an alternate method was applied using model compounds.

As an alternate approach, the ACDS β subunit K-edge was simulated by combining experimentally observed spectra of model compounds. As a square planar spectral component representing the distal M_b site, we used the previously published Ni K-edge data for the A-cluster in the isolated CODH/ACS α subunit.[14] The spectrum of the tetrahedral compound PhTt(*t*Bu)-NiCl was used for the contribution from the proximal site M_a. When these two spectra were averaged, the resulting spectrum had an overall shape that fit the experimental data for the ACDS β subunit significantly better than the FEFF8 calculations (Figure 4, right **c**+**d**). In particular, there was better agreement in the region around the 8349 eV peak. However, the combined spectrum had a stronger "1s → 3d" transition, with a weaker "1s → $4p_z$" transition.

A simulation then was carried out using the reported spectrum for 1,10 phenanthroline treated α subunit as the square planar component. In this case, using 60% α subunit and 40% PhTt-(*t*Bu)NiCl, the agreement near 8349 eV was excellent (Figure 4, right **c**+**e**). The intensity of the "1s → 3d" transition also showed a better match, but the "1s → $4p_z$" intensity was still lower than observed. The N_2S_2 coordinated distal Ni site also could be mimicked, without using protein crystallographic data, by employing the square planar inorganic complex $(Bu_4N)[TrisFe_4S_4NiN_2S_2]$,[42] in combination with the tetrahedral compound PhTt(*t*Bu)NiCl, as shown in Figure 4, right **c**+**f**. In general, combinations of spectra for a square planar and a tetrahedral Ni capture the overall characteristics of the ACDS β subunit K-edge, and in certain cases fit very nicely several specific features as well. The fact that some discrepancies do remain might be an indication that the true geometries are distorted from strict D_{4h} and T_d symmetry.

Fe EXAFS Analysis. The Fe K-space EXAFS and Fourier transforms for as-isolated, Ti^{3+}-treated, and Ti^{3+}/CO forms of the ACDS β subunit are shown in Figure 5. In all cases, there are two major components, which correspond to Fe−S and Fe−Fe interactions. For the as-isolated form, the EXAFS spectrum can be simulated by 4 Fe−S at ∼2.30 Å and 3 Fe−Fe interactions at 2.74 Å, consistent with proposals for the presence of an $[Fe_4S_4]^{2+}$ cluster,[40,43] and similar to previous EXAFS results on the CODH/ACS α subunit (4 Fe−S at ∼2.30 Å and 3 Fe−Fe at 2.71 Å).[14] There was no obvious Fe−Ni interaction. Upon Ti^{3+} treatment, the average Fe−S distance expanded to 2.32 Å, and the Fe−Fe Fourier transform peak decreased in intensity. The latter effect can be modeled as a slight increase in the rms deviation (σ) of Fe−Fe distances, from ∼0.07 to 0.08 Å, indicating that the Fe−S cluster is slightly less symmetrical in the presence of Ti^{3+}.

For samples in which moderate edge shifts were observed (∼0.15 eV), the modest changes in the EXAFS are consistent with reduction to a $[Fe_4S_4]^{1+}$ species. However, at very low potentials, $[Fe_4S_4]$ clusters in some proteins, such as the nitrogenase Fe protein, can be reduced to an "all-ferrous" form.[33,44−46] Crystallographic analysis reported four Fe−Fe

(42) Riordan, C. G.; Mandimutsira, B. S. Personal communication.
(43) Lindahl, P. A.; Ragsdale, S. W.; Münck, E. *J. Biol. Chem.* **1990**, *265*, 3880−3888.
(44) Watt, G. D.; Reddy, K. R. N. *J. Inorg. Biochem.* **1994**, *53*, 281−294.
(45) Angove, H. C.; Yoo, S. J.; Burgess, B. K.; Munck, E. *J. Am. Chem. Soc.* **1997**, *119*, 8730−8731.

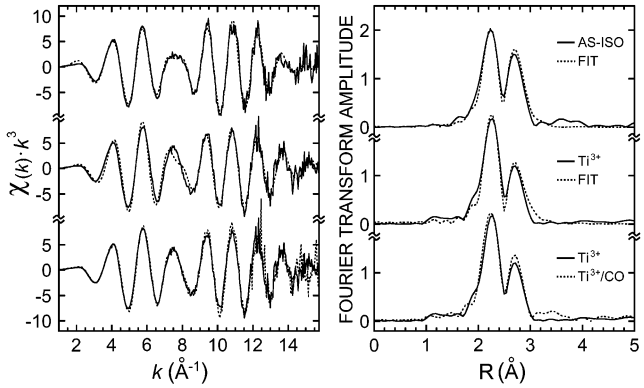

Figure 6. Ni *k*-space EXAFS and Fourier transforms for the ACDS β subunit. (Left) EXAFS spectra (—) and best fits (- - -) for samples: as-isolated, top; Ti^{3+} reduced, middle; and Ti^{3+}/CO treated, bottom. (Right) Fourier transformed EXAFS spectra (—) and best fits (- - -) of the as-isolated, top; and Ti^{3+} reduced samples, middle. The Ti^{3+} reduced (—) and Ti^{3+}/CO treated forms (- - -) are compared, bottom. The Fourier transform range was $k = 1-16.0$ Å^{-1}.

Table 1. Fe and Ni Coordination Parameters of the ACDS β Subunit from EXAFS Fitting Analyses

sample	edge	C.N.	R (Å)	$\sigma^2(10^{-3}$Å$^2)$	F
as-isolated	Fe	4S	2.30	3.95	350.3
		3Fe	2.74	4.47	
Ti^{3+}-reduced	Fe	4S	2.32	3.41	403.5
		3Fe	2.74	6.36	
as-isolated	Ni	2.5S	2.18	3.29	407.9
		1.5N	1.90	4.50	
	Ni	2.5S	2.19	3.08	186.6
		1.5N	1.89	5.32	
		1Ni	2.96	7.37	
	Ni	2.5S	2.19	3.07	201.7
		1.5N	1.89	5.20	
		6C	2.99	6.06	
Ti^{3+}-reduced	Ni	2.5S	2.18	3.32	205.2
		1.5N	1.87	5.12	
		1Ni	2.97	4.11	
		0.5Fe	2.80	2.50	

distances greater than 2.65 Å and two less than 2.57 Å,[39] and prior EXAFS analysis of the Fe protein all-ferrous $[Fe_4S_4]^0$ cluster showed a 65−75% reduction of the Fe−Fe Fourier transform peak because of this cluster distortion.[33] In our experiments, one sample of the Ti^{3+}-reduced β subunit was obtained that showed a significantly lower Fe−Fe peak, even further reduced than shown in Figure 5, consistent with formation of an all-ferrous state $[Fe_4S_4]^0$. This sample also exhibited the lowest acetyltransferase activity of all, around 13%. Loss of activity of the isolated β subunit has been described previously at very low redox potentials.[7] Therefore, these findings suggest that conversion of the cluster to the all ferrous state $[Fe_4S_4]^0$ may be connected to activity loss.

EXAFS fitting results for the Ti^{3+}/CO form gave an average Fe−S distance of 2.31 Å, mid-way between the as-isolated and the Ti^{3+}-reduced samples (Figure 5, bottom panel). The rms deviation (σ = 0.075 Å) of the Fe−Fe distances also was intermediate between the as-isolated and Ti^{3+}-reduced states. This indicated less disorder in the $[Fe_4S_4]$ cluster and less reduction of the cluster by Ti^{3+} when the reaction was carried out in the presence of CO.

Ni EXAFS. The Ni K-space EXAFS and Fourier transforms for as-isolated, Ti^{3+}-treated, and Ti^{3+}/CO forms of the ACDS β subunit are shown in Figure 6. In all of these, the Fourier transform is dominated by a Ni−S component at ∼2.2 Å, along with a shorter distance shoulder from Ni−N/O components at ∼1.9 Å. The spectra were simulated at first using a variety of Ni−S and Ni−N combinations assuming integer coordination numbers (see Supporting Information). The fits using 2 Ni−S and 2 Ni−N gave lower *F* values than those with 3 Ni−S and 1 Ni−N; however, they also produced unreasonably high values for the Debye−Waller factor for the Ni−N shell ($\sigma^2 = 0.006-0.007$ Å^2) that do not agree with the values of ($\sigma^2 < 0.0045$ Å^2) found in model compound studies with Ni−N distances in the range around 1.9−2.0 Å.[47] Thereafter, on the basis of the evidence for separate Ni sites with different coordination environments, we modeled the EXAFS using an average of the proximal M_a and distal M_b sites with average Ni coordination by 2.5 S and 1.5 N. The subsequent fit yielded lower, more reasonable values for the Ni−N shell Debye−Waller factor, with average Ni−S and Ni−N/O distances of 2.18 and 1.90 Å respectively (Figure 6, Table 1). The optimized σ-values of 0.06 and 0.07 Å respectively, were still slightly larger than expected for thermal motion alone (∼0.05 Å),[37] indicating some static spread in both distances.

Ni EXAFS Long-Range Interactions. In the Fourier transform of the Ni EXAFS of the as-isolated protein, the third largest peak occurs at ∼3.0 Å. Possibilities include Ni−Fe or Ni−Ni interactions; however, Ni−Fe appears unlikely on the basis of the CODH/ACS crystal structure data in which M_a−Fe distances of 3.26−3.54 Å are present in forms of the A-cluster containing Cu at the proximal site[15] and 3.75 Å is indicated for the form containing Zn,[16] values that are too large to account for the ∼3.0 Å peak. The third form, in which Ni is located in both sites, had an Fe−Ni_a distance of 2.66 Å, which is substantially less than the ∼3.0 Å feature observed in the β subunit. The ∼3.0 Å feature is also in the region where second shell Ni−C interactions might be observed, especially from the peptide backbone of deprotonated amide groups acting as ligands to the distal Ni. From the EXAFS alone, it is difficult to assign this 3.0 Å feature; however, if we examine the distribution of Ni−C distances around the Ni sites in the protein crystal structures, an average distance of 2.94 Å is found for the 6 shortest Ni−C distances, with an rms deviation of 0.08 Å. Given this degree of variation in combination with thermal motion, the resultant Debye−Waller factor would markedly attenuate the Ni−C EXAFS, resulting in a much smaller feature. Therefore, a Ni−C interaction is a less likely explanation of the 3.0 Å peak.

Curve-fitting analysis using a model that incorporates a Ni−Ni interaction resulted in substantially lower *F* values than could be obtained in the absence of a Ni−Ni term, and a value of 2.96 Å was found for the Ni−Ni distance (Figure 6, Table 1). This value agrees within experimental error for crystal structures at the current resolutions (1.9−2.2 Å)[15,16] with M_a−Ni_b distances ranging from 2.83 to 3.04 Å in two different A-cluster forms in one report,[16] and with the value of 2.82 Å found for the Cu−Ni_b distance in the other.[15] Furthermore, the 2.96 Å value would not agree with Ni−Fe distances seen in the crystal structures,

(46) Strop, P.; Takahara, P. M.; Chiu, H.-J.; Angove, H. C.; Burgess, B. K.; Rees, D. C. *Biochemistry* **2001**, *40*, 651−656.
(47) Maroney, M. J.; Colpas, G. J.; Bagyinka, C.; Baidya, N.; Mascharak, P. K. J. *Am. Chem. Soc.* **1991**, *113*, 3962−3972.

Scheme 1. Working Model of the Structure of the A-Cluster in the ACDS β Subunit

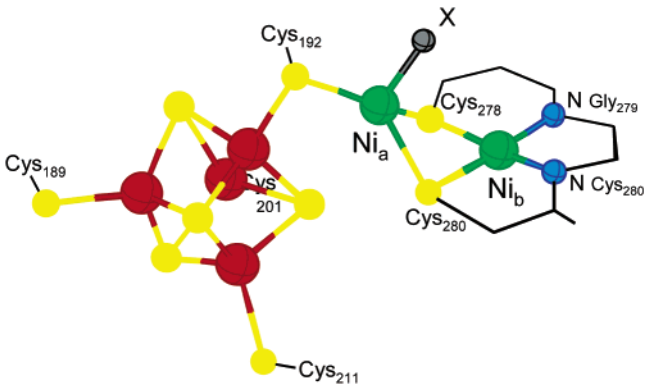

which are either significantly longer or shorter, and therefore, a Ni−Ni interaction is proposed.

For the Ti^{3+}-treated enzyme, the Ni−S, Ni−N/O, and 3.0 Å features all persist, and another peak appears at ∼2.7 Å (Figure 6 right, middle panel). The Ni EXAFS for the Ti^{3+}/CO sample was similar except that the ∼2.7 Å peak was stronger, while the 3.0 Å feature was somewhat less intense (Figure 6 right, bottom panel). The new ∼2.7 Å feature might represent an alternate Ni−Ni distance, a Ni−C interaction, or a new Ni−Fe distance. For the latter case, we have modeled the EXAFS as an average of 2.5 Ni−S, 1.5 Ni−N/O, 1 Ni−Ni, and 0.5 Ni−Fe components (Table 1). The Ni−Fe distance predicted from the fit was 2.80 Å, which is still somewhat larger than the 2.66 Å value found for A-cluster form containing distorted square planar Ni at the proximal site,[16] but is similar to the Ni−Fe distances found from recent crystallographic studies on the CO dehydrogenase C-cluster, an Ni−Fe_4S_{4-5} arangement in which several Ni−Fe distances exist in the range from 2.6 to 2.9 Å.[26,48] The appearance of this 2.8 Å feature could be due to a rearrangement of the A-cluster upon reduction of the [Fe_4S_4] center by Ti^{3+} citrate. Geometric changes were indicated in the [Fe_4S_4] cluster upon reduction, and these changes potentially could be related to rearrangement of the [Fe_4S_4] cluster, as a basis for the appearance of a Ni−Fe interaction.

Conclusions

The results presented here support a working model of the β subunit A-cluster consisting of an [Fe_4S_4] cluster bridged to a binuclear Ni−Ni site with substantially different geometries at each of the Ni centers (Scheme 1). A stoichiometric arrangement of [Fe_4S_4]−Ni−Ni was indicated for the ACDS β subunit A-cluster based on the 2:1 Fe:Ni ratio (and the absence of significant levels of other metals, including Cu and Zn) found for both the recombinant protein used in these studies, and for the native subunit isolated from the ACDS complex.[8] The standardized Ni/Fe K fluorescence ratios measured here agree with this assignment of stoichiometry.

Using two approaches to model the Ni XANES spectrum of the as-isolated β subunit (one with experimentally measured model compounds of known geometries and the other on the basis of theoretically calculated spectra) we found that the Ni K-edge was best represented as being composed of two separate signals, one arising from a square planar Ni site, and the other due to a Ni site in tetrahedral or distorted tetrahedral geometry. The Ni XANES and EXAFS of the ACDS β subunit showed some resemblance to previously reported spectra for the α subunit from CODH/ACS.[14] We note that the spectrum of the β subunit corresponds somewhat better with the 1,10-phenanthroline-treated CODH/ACS α subunit. However, the phen-extracted α spectrum exhibits more intensity in the 8349 eV region, which we assign to tetrahedral Ni. It was assumed that phen selectively removes the tetrahedral species, leaving behind distal square planar Ni. Nonetheless, proximal tetrahedral Ni has been considered to correspond to a "closed'" protein conformation, while proximal square planar Ni would exist in the "open" conformation. Therefore, the "lability" of the proximal Ni may reflect solvent accessibility as opposed to the Ni geometry per se (as mentioned in ref 16). Notwithstanding, the best simulations of the ACDS β subunit still required addition of from 40 to 50% of a purely tetrahedral component, reasonably well-served by the model compound PhTt(*t*Bu)NiCl.

All of the A-cluster spectra exhibit a combination of Ni−S and Ni−N/O components in the EXAFS and a relatively strong "1s → $4p_z$" feature in the XANES. The "1s → $4p_z$" feature has been assigned to a distorted square planar Ni site,[14,20] and it presumably derives some (or all) of its intensity from the distal square planar Ni_b species observed in all of the crystal structure A-clusters.[15,16] In the structure of Darnault et al.,[16] the proximal site, M_a, is predominantly distorted square planar when occupied by Ni, and thus the question arises − are both Ni species best described as distorted square planar Ni(II)? Our simulation of the XANES region of the ACDS β subunit suggests that a significant fraction of the Ni is better described by a tetrahedral or distorted tetrahedral geometry. This complements our finding from L-edge spectroscopy that approximately one-half of the Ni can be simulated by a high-spin Ni(II) species.[23] It is difficult to reconcile completely these results with the Ni_a geometries found in the crystal structures, given that the proximal site was only partially occupied by distorted square planar Ni with the remaining α subunit containing a tetrahedral Zn.[16] Since this structure was solved using crystals prepared by long-term incubation in the presence of dithionite, a non-innocent reductant that could have provided an additional ligand to Ni, it seems plausible that the relative population of distorted square planar and tetrahedral Ni in our samples differs from the diffraction result.

The Fe XANES and EXAFS were consistent with the presence of a [Fe_4S_4]$^{2+}$ cluster and indicated that reduction to the [Fe_4S_4]$^{1+}$ state takes place upon treatment of the β subunit with Ti^{3+} citrate. In the most strongly reduced sample, evidence suggests a [Fe_4S_4]^0 oxidation level, similar to that which can be achieved in the nitrogenase Fe protein. Reduction to this state correlated with substantial losses of acetyltransferase activity. Such losses might be accounted for by a mechanism in which the β subunit acetyl-enzyme species forms in an oxidative addition reaction. In such a mechanism, reduction of the acetyl-enzyme species under strongly reducing conditions would prevent the reverse reaction of reductive elimination needed to complete the acetyl transfer reaction cycle. Under milder reduction conditions, in which a majority of the activity was maintained, the Fe EXAFS results indicated a slight expansion of the Fe−S "cube". A Ni−Fe interaction was suggested in the reduced enzyme by Ni EXAFS; however, no

(48) Drennan, C. L.; Heo, J.; Sintchak, M. D.; Schreiter, E.; Ludden, P. W. *Proc. Natl. Acad. Sci. U.S.A.* **2001**, *98*, 11973−11978.

obvious Ni−Fe component could be seen in the Fe EXAFS − a result that simply may be due to the inability to detect such a signal in the case that only 1 of 4 Fe atoms would be in the vicinity of a Ni.

The Ni K-edge spectrum of the β subunit was less strongly influenced than the Fe-edge by reduction with Ti^{3+}. However, the effects suggested that a fraction of at most 50% of the Ni(II) present in the as-isolated enzyme could be reduced to a Ni(I) state. This result agrees with the L-edge and XMCD studies in which approximately one-third of the Ni was converted to a species assigned to Ni(I).[23]

A unique Ni K-edge spectrum was found for the enzyme treated with Ti^{3+} citrate in the presence of CO, which was distinct from that of the as-isolated enzyme and from that of the enzyme in the presence of Ti^{3+} citrate alone (Figure 2B). Absorption from two separate Ni sites again would be expected to contribute to the spectrum of the enzyme in the Ti^{3+}/CO form, and the resulting spectrum can be interpreted further in view of the findings from the accompanying L-edge and XMCD studies.[23] In those experiments a major high-spin Ni(II) component, observed in the as-isolated β subunit and corresponding to roughly one-half of the total Ni, was converted essentially completely to a low-spin Ni(II) form observed in the Ti^{3+}/CO treated enzyme. Thus, changes that take place upon reaction at the site containing high-spin Ni(II) also may be responsible mainly for the characteristic changes observed in the Ni K-edge spectrum of the Ti^{3+}/CO form. Overall, the evidence suggests that the K-edge spectral changes occur primarily in only one of the underlying components that would contribute about one-half of the total spectrum. This would correspond to the proximal tetrahedral Ni site, which is present as high-spin Ni(II) in the as-isolated enzyme, but is converted to a low-spin Ni(II) form, detectable upon reaction with CO in the presence of Ti^{3+} citrate.

The Ni EXAFS results can be reasonably fit using non-integer coordination numbers of 2.5 S and 1.5 N/O (Figure 6, Table 1), which are the average coordination numbers in the A-cluster structure shown in Scheme 1. The significant feature at ∼3.0 Å in the Ni EXAFS cannot be unambiguously assigned on the basis of the spectroscopic data alone. However, distance data from recent crystal structures indicate the most likely explanation for the ∼3.0 Å peak is due to Ni−Ni interaction. Upon reduction of the enzyme an additional feature is observed at ∼2.7 Å. Although a shortened Ni−Ni distance cannot be excluded, this peak is tentatively assigned as a new Ni−Fe distance, and fit to 0.5 Ni−Fe at 2.80 Å. Various possible rearrangements of the A-cluster can be considered, such as movement of the proximal Ni so that it approaches the $[Fe_4S_4]$ cluster, either with or without an increase in the Ni−Ni distance. These results emphasize further the need to consider different protein conformational states for the effects they may have on the coordination environments of individual metals in the A-cluster.

Acknowledgment. We thank Drs. E. I. Stiefel and K. Wang for the $(Bu_4N)Ni(tfd)_2$ sample, Professor C. G. Riordan for the PhTt(*t*Bu)NiCl sample, and Dr. D. J. Evans for the [Fe{$N(CH_2CH_2S)_3$}(NO)NiCl(dppe)] sample. We are indebted to Professor B. Friedrich, Professor C. L. Drennan, and Professor S. W. Ragsdale, for providing samples of *R. eutropha* hydrogenase, crystalline *R. rubrum* CODH, and *M. thermoacetica* CODH/ACS, respectively. We acknowledge Professor J. Rehr for advice about FEFF8 calculations and Dr. H.-X. Wang and the SSRL biotech staff for their help with the beam lines. This work was supported by NIH Grants GM-44380 and GM-65440 (S.P.C.), NSF Grant MCB-0215160 (D.A.G.), the U.S. Department of Energy Grant DE-FG02-00ER15108 (D.A.G), and the U.S. Department of Energy, Office of Biological and Environmental Research. SSRL is supported by the U.S. Department of Energy, Office of Basic Energy Sciences.

Supporting Information Available: Table of Ni EXAFS fitting results using integer coordination numbers (Table S1), and figure showing persistence of the ∼3.0 Å feature regardless of *k* range used in Fourier transformations (Figure S1) (PDF). This material is available free of charge via the Internet at http://pubs.acs.org.

JA036602A